Near-infrared transparent conductive electrodes based on composite GaAs-metal deep sub-wavelength high contrast grating

Natan Monvoisin, Weronika Glowadzka, Franck Carcenac, Stéphane Calvez, Olivier Gauthier-Lafaye, Antoine Monmayrant, Marcin Gebski, Tomasz Czyszanowski, Guilhem Almuneau

Near-infrared transparent conductive electrodes based on composite GaAs-metal deep sub-wavelength high contrast grating

Natan Monvoisin[1], Weronika Głowadzka[2], Franck Carcenac[1], Stéphane Calvez[1], Olivier Gauthier-Lafaye[1], Antoine Monmayrant[1], Marcin Gębski[2], Tomasz Czyszanowski[2], and Guilhem Almuneau[1,*]

[1]LAAS-CNRS, Université de Toulouse, CNRS, INSA, 31400 Toulouse, France
[2]Technical University of Łódź, Laboratory of Photonics Institute of Physics, 90-924 Łódź, Poland

E-mail: *almuneau@laas.fr

8 November 2024

Abstract. This paper demonstrates the fabrication of near-infrared transparent electrodes customized for specific light polarization. We achieve this by employing semiconductor deep subwavelength monolithic high-contrast gratings (MHCG) integrating metal stripes. Through the combination of GaAs-based MHCG with TiAu or Au stripes within a deep sub-wavelength grating, polarization selective transmission exceeding 80% over a wide spectral range is achieved for structures designed to operate around a wavelength of 940 nm for either TE or TM excitation. At maximum 85% transmission is reached which relates to 122% transmission with respect to the transmission through plain GaAs-air interface. Additionally, these structures exhibit low sheet resistance ($1.4\,\Omega/sq$). Hybrid metal-stripes/MHCG grating (MetalMHCG) enables record-breaking polarized light transmission and electrical conductivity simultaneously. Our work represents the first demonstration of MetalMHCG in the near-infrared range, thanks to an advanced nanofabrication process of this sub-λ hybrid semiconductor/metal grating, showing optical and electrical properties not seen in alternative transparent conductive electrode designs. The proposed approach has the potential to enhance electrical injection uniformity in optoelectronic devices such as LEDs, semiconductor lasers and photodetectors.

Submitted to: *J. Phys. : Photonics*

1. Introduction

Optoelectronics technology relies on transparent conductive electrodes (TCEs) enabling current flow within the electrode plane and transmittance of light through the TCE. Achieving high conductivity in TCEs necessitates a high concentration of free carriers, which simultaneously limits their transmittance. This inherent trade-off between

electrical conductivity and light transmission has been extensively investigated and is widely recognized in the field of TCEs for visible spectrum (VIS) applications [1,2]. The utilization of TCEs in applications related to near infrared spectrum is of heightened difficulty as transmission is deteriorated by increased absorption and reflection of TCEs. In the near infrared spectrum, the primary application of TCEs lies in their integration with optoelectronic devices such as LEDs, photodetectors (PDs), lasers, etc [3–5]. This integration aims to increase the performance of the devices, but it poses significant challenges. The main challenge arises from the resonance frequency of the free electron plasma which is located in the infrared spectrum. Enhanced interaction of the electromagnetic field with free electrons increases absorption and reflection, reducing the properties of conventional TCEs. In most of the demonstrations, TCEs were typically deposited on glass or polymer substrates with a refractive index ranging from 1.2 to 1.7, resulting in transmittance levels of 80% to 95% in the VIS [6] and 70% in the IR [7]. However, the transmission through the interface between air (refractive index of 1) and semiconductors (refractive index of 2.5 – 3.5) is typically limited to less than 80% in the case of wide bandgap and 70% in the case of narrow bandgap semiconductors.

Surpassing the transmission limit dictated by the Fresnel formula (which we call the Fresnel limit T_{FL}):

$$T_{FL} = 1 - \left(\frac{n-1}{n+1}\right)^2 = \frac{4n}{(n+1)^2} \tag{1}$$

(where n is the refractive index of the substrate and refractive index of air is assumed to be unity) represents a considerable achievement, posing a significant challenge for TCEs, particularly those implemented on semiconductors.

We define relative transmission (T_{rel}) as ratio between absolute transmission and Fresnel limit. For nearly all examples, TCEs exhibit lower transmission than the Fresnel limit, attributed to the reflection and absorption they introduce. Consequently, if these TCEs are deposited on a semiconductor surface, their transmittance is anticipated to be lower by approximately 15-25% compared to their transmission when deposited on low refractive index substrates. To address the inherent trade-off between conductivity and transmittance in TCEs, one can use a design that decouples the optical and electrical functionalities such as in [8–10], or by other means including the use of hybrid semiconductor MHCG combined with metal stripes [11]. In the latter case, referred hereafter as MetalMHCG, two configurations can be used: a first one where the metal stripes are positioned between the semiconductor stripes, referred to as the *bottom configuration* or B-TE (as illustrated in Figure 1a), and a second version where the metal stripes are located on top of the semiconductor stripes, termed the *top configuration* or T-TM (depicted in Figure 1b). As introduced in [12], in the deep sub-wavelength regime i.e. when $\lambda > n\Lambda$ (where Λ is the period of the MetalMHCG, λ – wavelength, n – refractive index of semiconductor), the grating forms a low-quality factor etalon, limited by the interface between MetalMHCG and air on one side and MetalMHCG and a homogeneous cladding layer on the other. The numerical analysis showed that TE-polarized light (for which the electric field vector is parallel to the

grating stripes) primarily resonates in the semiconductor stripes, while TM-polarized light (for which the magnetic field vector is parallel to the grating stripes) resonates within the air regions between semiconductor stripes (see Figure 1b). The difference in field distribution implies preferential metal position, at the bottom of the semiconductor grooves in the case of TE polarized light and on top of the semiconductor stripes in case of TM polarization (and thereby the short names introduced above). Experimental demonstrations of these TCEs were obtained for a wavelength of 4.5 µm in [13,14], where the T-TM (respectively B-TE) configuration exhibited 90% (resp. 92%) transmittance with a corresponding sheet resistance of $2\,\Omega/sq$ [13] (resp. $0.5\,\Omega/sq$ [14]). T_{rel} of both configurations are 130% and 133%, respectively.

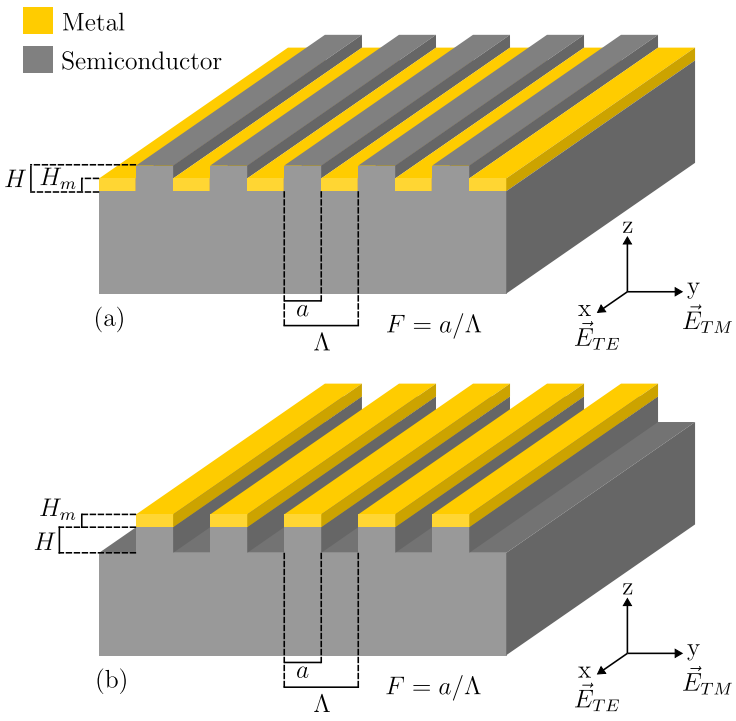

Figure 1: MetalMHCG configuration allowing high transmission of (a) TE polarization (B-TE), and (b) TM polarization (T-TM). Λ is the grating period, a the semiconductor stripe width, F the grating fill-factor, H the semiconductor stripe height, and H_m the metal stripe height.

Unlike conventional transparent electrodes such as ITO, this metalMHCG configuration allows both transparency, controlled by the optical properties of sub-wavelength gratings that can be shaped in terms of wavelength and polarization, and very low-resistance electrical conduction via a network of metallic grids. These advantages provide a dual benefit for vertical geometry components (LEDs, VCSELs, and photodetectors): improved lateral conduction and distribution of injected or generated current over larger surfaces, and minimized or even eliminated impact of the transparent electrode's optical properties on the component's performance. Consequently, applying metalMHCG to components in the near-infrared range could

enable higher current densities and, for emitters, ensure better control of the emitted beam, particularly in terms of polarization stability.

In this work, we extend the numerical and experimental study of MetalMHCGs to the near-infrared region. We confirm the working principles of such structures through the calculation of the optimal parameters to achieve high transmission using MetalMHCG high transmission for a wavelength range from 900 to 985 nm and normal incidence. We subsequently report and discuss the fabrication and the optical and electrical characterization of both B-TE and T-TM TCE structures on GaAs substrates.

2. Design of transparent MetalMHCG structures

The targeted MetalMHCG structures studied here are derived from optimal points in the transmission maps presented in Figure 2 that were obtained by numerical simulations based on the Rigorous Coupled-Wave Analysis (RCWA) method with the number of harmonics set to 50. The refractive index data of GaAs [15], Au [16], and Ti [17] which was used in the calculations include the dispersion. These maps illustrate the transmission at 940 nm for bottom normal incidence, varying the grating period Λ and semiconductor grating height H, while setting the titanium and gold layers heights respectively at 5 and 50 nm to correspond to the standard ohmic contact stack on p-doped GaAs. Grating fill-factors F of 0.4, 0.5, and 0.6 are presented, showcasing an important trade-off for technological fabrication. While achieving $F = 0.5$ is easier at such small periodicity, $F = 0.6$ and $F = 0.4$ enables a larger periodicity for high transmission, respectively in the B-TE and T-TM configurations.

Figure 2 shows theoretical transmission levels exceeding 95% for both MetalMHCG configurations, within the geometric parameter range accessible with standard nano-fabrication technology. These structures are tunable by adjusting parameters such as Λ, H, H_m, and F using a specified high refractive index substrate and metal.

Six structures have been selected from the aforementioned maps for subsequent experimental investigations. Their details are summarized in Table **??** in supplementary document providing their optimal parameters and theoretical transmission for the relevant polarization at 940 nm. While the calculated transmission and reflection spectra for these structures in a broader range are not shown here, they show that the high-transmission spectral window of T-TM is broader than that of the B-TE configuration. Despite this, the transmission behavior of B-TE also presents a relatively large window of about 200 nm, with transmission levels consistently above 80%.

When considering a GaAs/air interface, the Fresnel equation predicts a transmission value of approximately 70%, significantly lower than the theoretical transmission through MetalMHCG. As a result, these structures provide a metallic contact on one side and optical impedance matching on the other. In contrast to conventional TCEs, they offer high transparency while retaining the excellent electrical conductivity of metals. In the B-TE configuration, there is greater flexibility in choosing the composition of the metallic contact, as the transmission mechanism limits the interaction between light

and metal. This flexibility may be advantageous, especially in applications where an ohmic contact is necessary, like for LEDs, detectors or lasers. Additionally, the optimal periodicity is 35% larger than that in the T-TM configuration, concomitant with the use of larger metal lines for improved electrical conductivity and facilitating a more straightforward fabrication process.

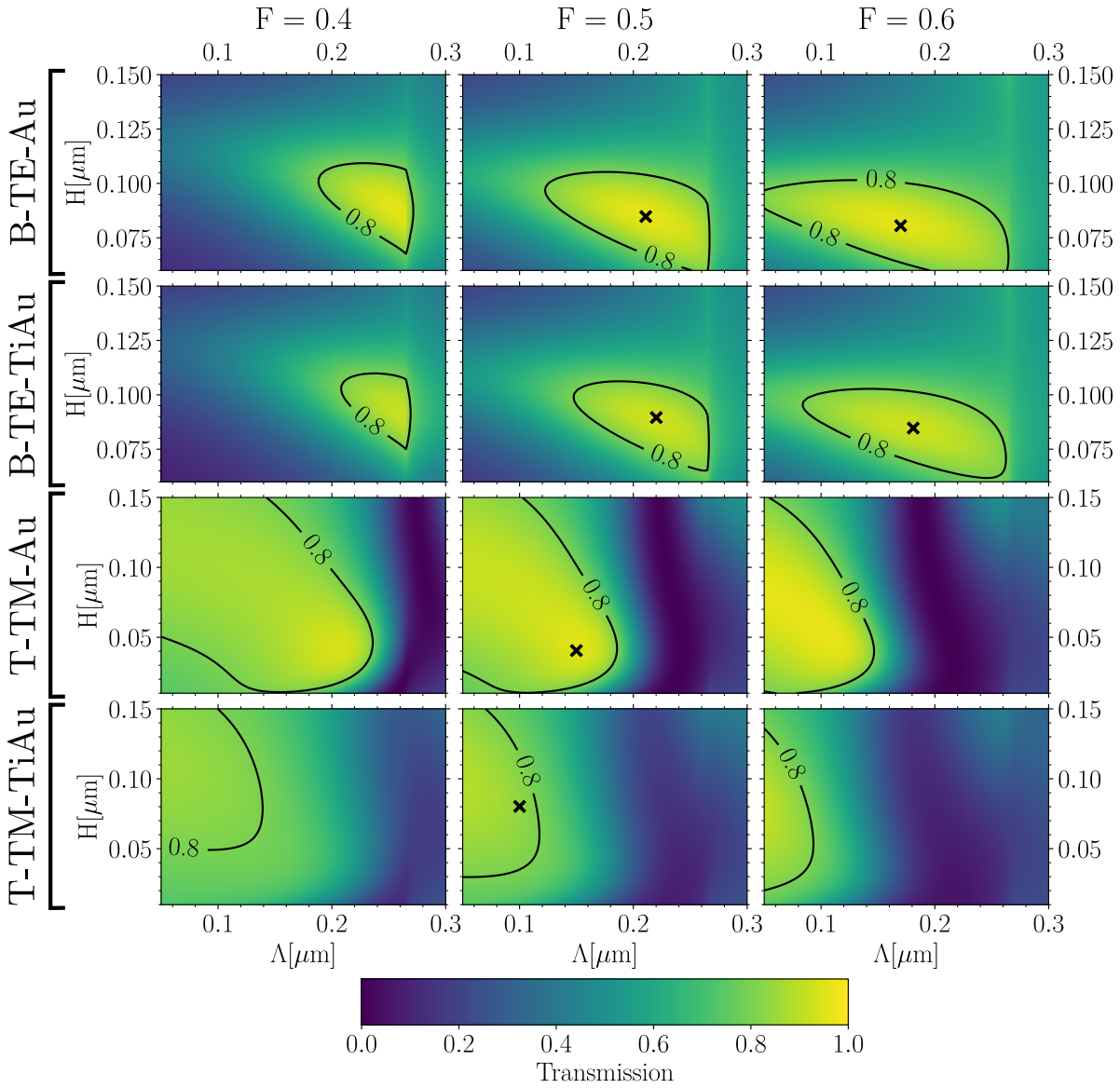

Figure 2: Transmission maps computed using RCWA for a wavelength of 940 nm at normal incidence, varying the semiconductor grating height H and period Λ. The metal thickness is fixed at 50 nm for gold (Au) and 5/50 nm for titanium/gold (Ti/Au) contact. Each line of the array plot represents the different studied configurations and crosses refer to the structures fabricated in this work (see table **??**). Each column corresponds to different grating fill-factor values: $F = 0.4$, $F = 0.5$, and $F = 0.6$.

3. Fabrication

In total, based on the structure designs summarized in table **??**, seven different samples were fabricated and then characterized to assess the impact of these geometric variables on the optical properties. Two series were fabricated, five samples following the B-TE configuration and two samples following the T-TM configuration, using manufacturing processes tailored to each configuration, as detailed in the supplementary document. For each series, two variants were used for the metal layer: Au, which represents the ideal configuration for this type of MetalMHCG structure for minimizing optical losses, and Ti/Au, which is more practical for component applications. In the latter case, Ti acts as an adhesion layer for Au on GaAs, while the Ti/Au combination forms a low-resistivity ohmic contact on doped GaAs.

For each B-TE and T-TM configuration, we varied the geometric parameters described before based on structures that were modeled and optimized for maximum transmission around 940 nm. Specifically, several sets of grating periods, fill factors, and etching depths of the semiconductor grating were used on different samples. In the supplementary document, the table **??** presents their respective measured dimensions and the associated uncertainties. Some representative examples of both the top- and cross-view scanning electron microscopy (SEM) images of the fabricated MetalMHCG structures are presented in Figures 3 and 4.

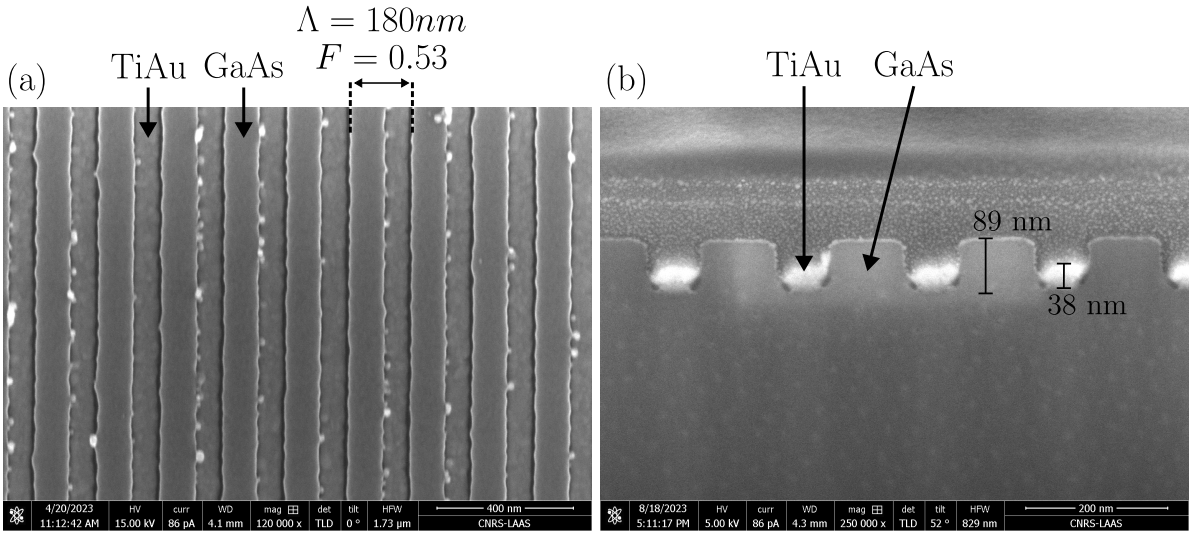

Figure 3: SEM images of the fabricated B-TE-TiAu-1 configuration: (a) top view from where grating period Λ and grating fill-factor F are measured, and (b) FIB-etched cross-section from where the GaAs teeth height H, the gold height H_{Au}, and the titanium height H_{Ti} are measured using vertical dimension scaling.

The periodicity of the metalMHCG grating is around a hundred nanometers, and the fabrication process—particularly the lift-off step (in the case of B-TM)—requires

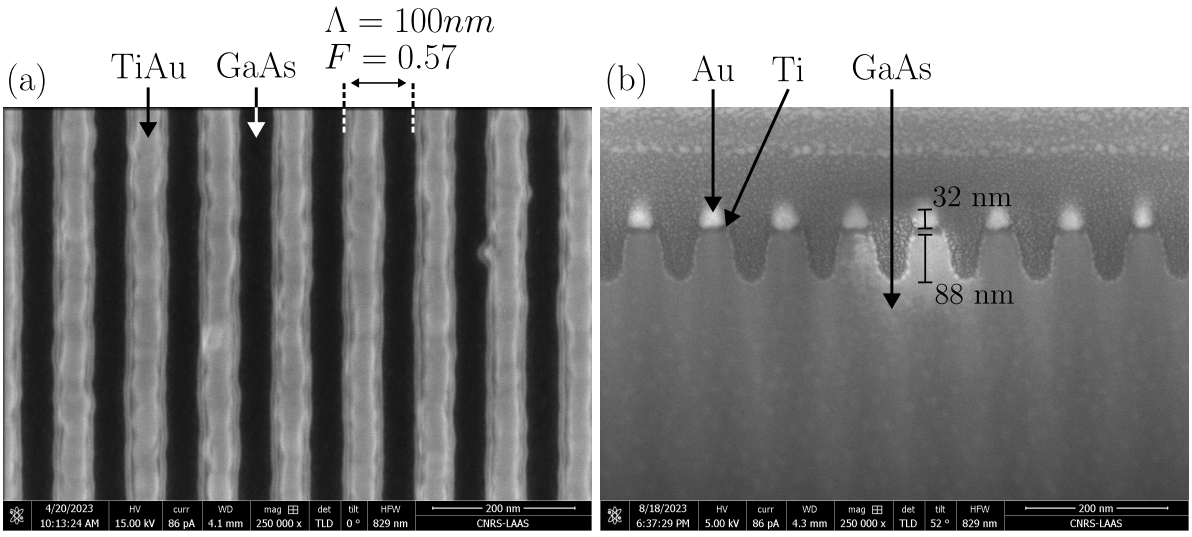

Figure 4: SEM images of the fabricated T-TM-TiAu configuration: (a) top view from where grating period Λ and grating fill-factor F are measured, and (b) FIB-etched cross-section from where the GaAs teeth height H, the gold height H_{Au}, and the titanium height H_{Ti} are measured using vertical dimension scaling.

special attention. To improve this lift-off step, the resist profile could be optimized with reverse single resist film or cap-shaped double layer resist. These changes may help eliminate the metallic residues observed on the edges of the grating lines. Additionally, another important area for enhancement is the reduction of the roughness of the grating lines through the optimization of the etching process.

4. Characterization

4.1. Optical spectroscopy

The fabricated MetalMHCG structures, as summarized in table **??**, were optically characterized using a dedicated spectroscopy setup (see Supplementary document). The structures were fabricated on one side of a double side-polished 625-µm-thick GaAs NID substrate and the laser beam used as optical source is focused on the sample surface with a waist estimated to ≃10µm, which is compatible with the fabricated structure size fo $40 \times 40\,\mu m^2$. Simulations confirms that the spectral response of the structures is not changed over the $\pm$ 2° of incidence induced by the beam waist at 940 nm.

The transmission spectra in both polarizations are presented in Figure 5 for the B-TE structures and Figure 6 for the T-TM structures. The measurements cover the 900-985 nm spectral range, corresponding to the wavelength tuning range of the laser source. Theoretical spectra calculated by RCWA using 50 harmonics are also presented taking into account averaged values for the geometric parameters and ideal straight-edged grating with rectilinear profiles.

While the calculated and measured curves generally align well, especially for polarizations with highest transmissions, the discrepancies can be attributed to the differences between the assumed profile geometry of the MetalMHCG and the actual profiles and the sidewall roughness produced during the fabrication process. In particular the calculated spectra do not take into account the uncertainties on the measured geometric parameters, this leading potentially to measured values exceeding theoretical ones.

Comprehensive transmission and reflection results under each polarization are depicted in Figures **??** and **??** of the supplementary document. At a wavelength of 940 nm, measured transmission, reflection, and losses (considered as the sum of absorption and uncollected scattering) are summarized in Table **??**, with losses calculated as $1 - T - R$.

These results illustrate the polarization-selective nature of the optical response, with B-TE structures primarily transmitting TE polarization and T-TM structures mainly transmitting TM polarization. Regardless of the metallic contacts (Au or TiAu), both configurations exhibit transmission levels above 80%, significantly surpassing the 70% GaAs/air plain interface Fresnel transmission, when considering the appropriate transmitted polarization, and showing the vanishing of the metal absorption which, without structuring, would represent a total shading surface of 50% to 60%.

Changing from Au to TiAu contact only marginally impacts the losses of the highly transmitted polarization. The lowest losses are observed in the T-TM configuration. The structure named B-TE-TiAu-2 exhibits the highest losses, possibly attributed to the metal residues remaining on the sides of the grating teeth after the lift-off step or imperfect grating dimensions and profile.

It should be made clear that the structures were fabricated on GaAs NID substrates and thereby present negligible free carrier absorption as compared to structures made on doped cap semiconductor layer as would be required to lower the Schottky barrier height and thereby obtain ohmic contacts. Nevertheless, assuming an absorption coefficient of $\sim 100\,\mathrm{cm}^{-3}$ as reported for p-GaAs doped at $1.6 \times 10^{19}\,\mathrm{cm}^{-3}$ [18] and considering layer thickness of 100 nm, the calculated additional absorption would increase by $\sim 0.1\%$, a value low enough to be confident that high transmission MetalMHCGs can also be obtained even with an ohmic contact.

Different types of defects are observed along the grating lines: local variations in GaAs stripes width due to vibrations during electron-beam lithography and the inherent impacts on etched edges profiles, metallic residues at the edges of the grating lines that can be minimized with an improved lift-off process, and erosion at the edges of metal lines used as an etching mask for the top configuration, which can be mitigated through protective layering. Despite the presence of these fabrication defects, it is noteworthy that the performance of metalMHCG in both configurations demonstrates excellent transparency properties, surpassing those of traditional TCE approaches. This observation suggests that the optical properties of metalMHCG exhibit strong resilience against irregularities introduced by the technological process.

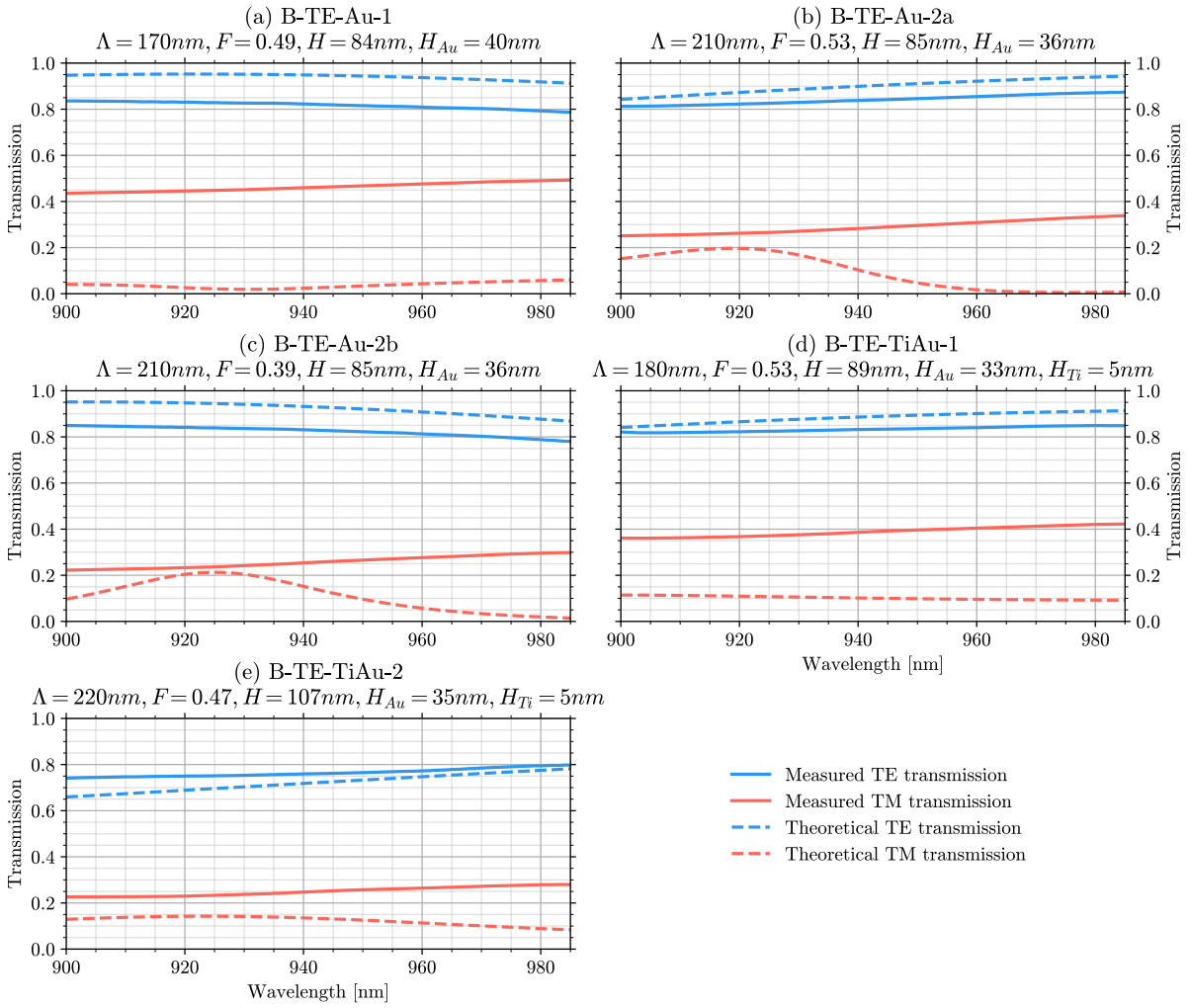

Figure 5: Comparison between measured and calculated spectral transmission of different fabricated B-TE MetalMHCG at normal incidence between 900 and 985 nm. For each structure, the grating dimensions are specified : the period Λ, the fill-factor F, the gallium arsenide height H, the gold height H_{Au}, and the titanium height H_{Ti}.

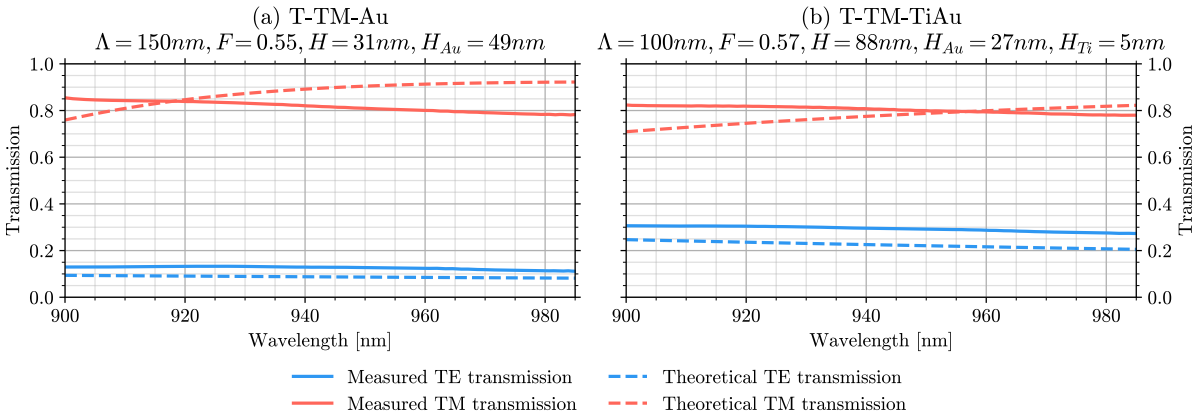

Figure 6: Comparison between measured and calculated spectral transmission of different fabricated T-TM MetalMHCG at normal incidence between 900 and 985 nm. For each structure, the grating dimensions are specified : the period Λ, the fill-factor F, the gallium arsenide height H, the gold height H_{Au}, and the titanium height H_{Ti}.

4.2. Electrical sheet resistance

To complement the optical characterization, we also measured the sheet resistance of an array of gold nanowires with dimensions closely matching those required in either the B-TE and the T-TM configurations.

The fabrication process for the specific samples used to measure electrical sheet resistance is detailed in the supplementary document. To characterize the lateral electrical access resistance of the metal grid over lengths up to 40 μm, the sample consists of several arrays of 1D gold stripes directly deposited on a planar NID GaAs substrate. The goal was not to characterize the direct ohmic injection into an active component, which would have required the complete development of a device fabrication process. Similarly to the MetalMHCG scaling geometry, a series of 60-nm-wide metal wires with a periodicity of 150 nm was used.

In this experiment, we measured the resistance of a set ranging from a single nanowire to several nanowires using a two-probe setup, and extracted the sheet resistance using the formula $R_{sh} = (R - R_p)N\frac{W}{L}$, where R is the measured resistance, R_p is the parasitic contacts and probes resistance measured in short circuit configuration, N is the number of nanowires, W is the nanowire width, and L is their length.

Figure 7 presents the measured R_{sh} with respect to the number of nanowires, including both 20-µm-long and 40-µm-long sets. The small decrease of sheet resistance between 1 and 10 nanowires is attributed to a slight increase of the metal thickness. This thickness is dependent of the patterned line width, which tends to increase with the proximity effects during the electron-beam lithography exposure. The results yield a measured mean value of $R_{sh} = 1.4 \pm 0.1\Omega/sq$ for a single nanowire, equivalent to a resistivity of $\rho = (6.7 \pm 0.5) \times 10^{-8}\Omega \cdot \mathrm{m}$. This resistivity is less than three times the bulk resistivity of gold, which is $2.44 \times 10^{-8}\Omega \cdot \mathrm{m}$. This demonstrates the excellent electrical conductivity of gold, even in the form of nanowires. Combined with high optical transmission results, this makes MetalMHCG structures very promising for implementation as electrodes.

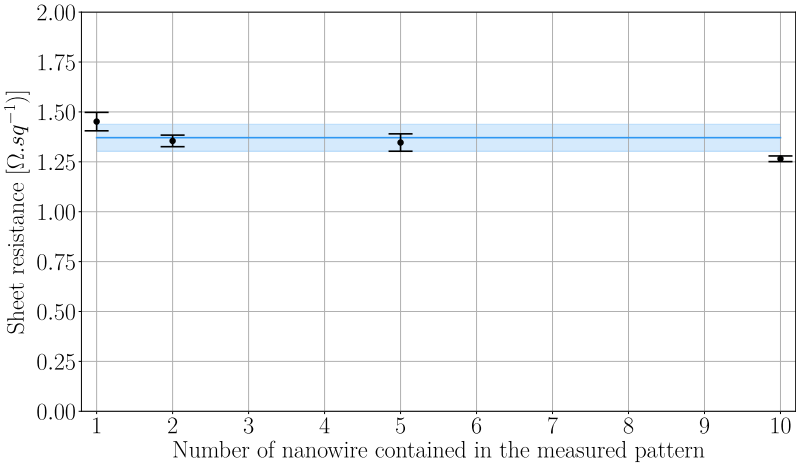

Figure 7: Sheet resistance measurement results as a function of the number of nanowire. The blue line is the mean value, and the light blue rectangle shows the standard deviation around the mean value.

Conclusion

In this research, we performed an experimental demonstration of a MetalMHCG operating in near-infrared spectral region in configurations where the metal stripes are implemented either between the semiconductor stripes (B-TE) or deposited on top of the semiconductor stripes (T-TM). We designed and fabricated several geometries and types of MetalMHCG operating around 940 nm, first by creating structures that work in both polarizations with B-TE and T-TM configurations. Among these two configurations, we compared two approaches for the metal layer: using a simple thin gold layer or implementing a Ti/Au bilayer, commonly used to achieve low-resistivity ohmic contacts on doped GaAs. Among the various fabricated sample variants, we also studied the influence of geometric parameters, such as the period in the 100-200 nm range, the depth of the deep sub-wavelength grating, and its fill factor. As described in [19], high transmittance is achieved by optimizing the grating design, enabling polarization-dependent light funneling and resonance coupling that minimizes metal absorption and Fresnel reflection.

The transmission of electrodes was examined in the experimental setup composed of tunable laser source in the wavelength range from 900 to 985 nm in which either signal was observed to vary slowly with wavelength. The transmission mechanism through the MetalMHCGs enabled transmittance of 82% and 84% of polarized light in B-TE and T-TM configuration, respectively, the relative transmission T_{rel} of 118% and 122% being never reported, to the best of our knowledge. Moreover, the presence of the titanium layer does not significantly modify the transmission. The measured values are however lower (by approximately 10%) than the optimized calculated values. This reduction could be caused by a combination of imperfect experimental grating profiles and parameters or by a mismatch between the modeled and experimental

optical properties of the metal involved. Numerical simulations taking into account the measured MetalMHCG cross-sections show closer correspondence to experiment (see Supporting Information). Remaining discrepancies can be attributed to non-perfect periodicity of MetalMHCG stripes. Additionally, the MetalMHCG in the B-TE configuration was observed to exhibit weaker polarization selectivity compared to the T-TM configuration as they respectively lead to 60% and 40% transmittance of unpolarized light.

The optical properties of MetalMHCG enable record high transmission due to the significant reduction of the interaction between the optical field and the metal stripes while maintaining sheet resistance of 1.4 Ω/sq. This value ranks among the lowest reported for a transparent electrode, even when considering highly conductive structures resulting from a strong trade-off between conductivity and transparency [3]. Direct comparison of these results with widely used TCEs can be found in Figure **??** in the supplementary document. To go even further, such MetalMHCG-type structure can also be designed as a polarization-independent TCE utilizing the B-TE configuration, as theoretically demonstrated in [19].

This work demonstrates the extension of the MetalMHCG approach into near-infrared applications. While MetalMHCGs have previously proven to be efficient transparent electrodes in the mid-infrared spectral range, this study pushes technological boundaries by realizing MetalMHCGs with periods as low as around 100 nm. Through experimental validation, we demonstrate exceptionally high transmission and record-low sheet resistance, emphasizing the robustness and flexibility of MetalMHCGs in the near-infrared window.

The integration of the metalMHCG interface as a transparent electrode in near-infrared components represents a significant advantage. Thanks to its great flexibility in shaping transparency properties and adapting them to the component, this integration enables access to applications requiring high current densities over large surfaces. When required, the extension of the nanostructuration capability to larger surfaces up to the millimeter or centimeter range, for which a tool such as nanoimprint lithography could be relevant, is the most challenging aspect of the integration. The devices studied around 940 nm here can be directly applied to large-area VCSELs for LIDAR applications, or to detection systems, enhancing spectral detectivity for photodetectors.

Acknowledgments

This research was funded by Agence Nationale de la Recherche TRAVEL M-ERA NET project ANR-20-MERA-0002. This work was partly supported by LAAS-CNRS micro and nanotechnologies platform member of the French RENATECH network.

References

[1] L.-H. Qin, Y.-Q. Yan, G. Yu, Z.-Y. Zhang, T. Zhama, and H. Sun, "Research progress of transparent electrode materials with sandwich structure," Materials, vol. 14, no. 15, 2021.

[Online]. Available: https://www.mdpi.com/1996-1944/14/15/4097

[2] A. Kumar, M. Kumar, M. Goyat, and D. Avasthi, "A review of the latest developments in the production and applications of ag-nanowires as transparent electrodes," Materials Today Communications, vol. 33, p. 104433, 2022. [Online]. Available: https://www.sciencedirect.com/science/article/pii/S2352492822012740

[3] K. Ellmer, "Past Achievements and Future Challenges in the Development of Optically Transparent Electrodes," Nature Photonics, vol. 6, no. 12, pp. 809–817, 2012.

[4] M. Morales-Masis, S. De Wolf, R. Woods-Robinson, J. W. Ager, and C. Ballif, "Transparent Electrodes for Efficient Optoelectronics," Advanced Electronic Materials, vol. 3, no. 5, p. 1600529, 2017.

[5] C. Chua, R. Thornton, D. Treat, V. Yang, and C. Dunnrowicz, "Indium Tin Oxide Transparent Electrodes for Broad-Area Top-Emitting Vertical-Cavity Lasers Fabricated Using a Single Lithography Step," IEEE Photonics Technology Letters, vol. 9, no. 5, pp. 551–553, 1997.

[6] X. Li, Y. Zhu, W. Cai, M. Borysiak, B. Han, D. Chen, R. D. Piner, L. Colombo, and R. S. Ruoff, "Transfer of large-area graphene films for high-performance transparent conductive electrodes," Nano Letters, vol. 9, no. 12, pp. 4359–4363, Oct. 2009.

[7] A. Anand, M. M. Islam, R. Meitzner, U. S. Schubert, and H. Hoppe, "Introduction of a novel figure of merit for the assessment of transparent conductive electrodes in photovoltaics: Exact and approximate form," Advanced Energy Materials, vol. 11, no. 26, p. 2100875, 2021. [Online]. Available: https://onlinelibrary.wiley.com/doi/abs/10.1002/aenm.202100875

[8] P. B. Catrysse and S. Fan, "Nanopatterned Metallic Films for Use As Transparent Conductive Electrodes in Optoelectronic Devices," Nano Letters, vol. 10, no. 8, pp. 2944–2949, 2010.

[9] Q. Guo Du, K. Sathiyamoorthy, L. Ping Zhang, H. Volkan Demir, C. Hin Kam, and X. Wei Sun, "A two-dimensional nanopatterned thin metallic transparent conductor with high transparency from the ultraviolet to the infrared," Applied Physics Letters, vol. 101, no. 18, Oct. 2012.

[10] N. K. Gupta, H. Wanare, and S. A. Ramakrishna, "Design of transparent conducting plasmonic metasurfaces and theory of impedance-matched metastructures," Plasmonics, vol. 15, no. 6, pp. 2109–2117, Jul. 2020.

[11] A. Cai and J. Tan, "A broadband transparent window in a continuous metal film coated with double layer hybrid dielectric gratings," Optics Communications, vol. 403, pp. 193–196, Nov. 2017.

[12] T. Czyszanowski, A. K. Sokół, M. Dems, and M. Wasiak, "Transparent Electrode Employing Deep–Subwavelength Monolithic High-Contrast Grating Integrated with Metal," Optics Express, vol. 28, no. 19, p. 28383, 2020.

[13] L. Y. M. Tobing, M. Wasiak, D. H. Zhang, W. Fan, and T. Czyszanowski, "Nearly Total Optical Transmission of Linearly Polarized Light through Transparent Electrode Composed of GaSb Monolithic High-Contrast Grating Integrated with Gold," Nanophotonics, vol. 10, no. 15, pp. 3823–3830, 2021.

[14] M. Ekielski, W. Głowadzka, K. Bogdanowicz, M. Rygała, M. Mikulicz, P. Śpiewak, M. Kowalski, M. Gębski, M. Motyka, A. Szerling, and T. Czyszanowski, "Monolithic high contrast grating integrated with metal: Infrared electrode with exceptionally high conductivity and transmission," Advanced Functional Materials, vol. n/a, no. n/a, p. 2312392, Dec. 2023. [Online]. Available: https://onlinelibrary.wiley.com/doi/abs/10.1002/adfm.202312392

[15] S. Adachi, "Optical dispersion relations for $GaP, GaAs, GaSb, InP, InAs, InSb, Al_xGa_{1-x}As, and In_{1-x}Ga_xAs_yP_{1-y}$," Journal of Applied Physics, vol. 66, no. 12, pp. 6030–6040, 12 1989.

[16] D. I. Yakubovsky, A. V. Arsenin, Y. V. Stebunov, D. Y. Fedyanin, and V. S. Volkov, "Optical constants and structural properties of thin gold films," Opt. Express, vol. 25, no. 21, pp. 25 574–25 587, Oct 2017.

[17] K. J. Palm, J. B. Murray, T. C. Narayan, and J. N. Munday, "Dynamic optical properties of metal hydrides," ACS Photonics, vol. 5, no. 11, pp. 4677–4686, 2018.

[18] B. Ullrich, S. R. Munshi, and G. J. Brown, "Photoluminescence Analysis of P-Doped GaAs Using

the Roosbroeck–Shockley Relation," Semiconductor Science and Technology, vol. 22, no. 10, pp. 1174–1177, 2007.

[19] A. K. Sokól and T. Czyszanowski, "Nearly Perfect Transmission of Unpolarized Infrared Radiation through a One-Dimensional Metal Grating Embedded in a Monolithic High-Contrast Grating," Optics Express, vol. 28, no. 26, p. 38857, 2020.